



THE UNIVERSITY *of* EDINBURGH

Edinburgh Research Explorer

Impacts of relative permeability hysteresis, wettability, and injection/withdrawal schemes on underground hydrogen storage in saline aquifers

Citation for published version:

Pan, B, Liu, K, Ren, B, Zhang, M, Ju, Y, Gu, J, Zhang, X, Clarkson, CR, Edlmann, K, Zhu, W & Iglauer, S 2023, 'Impacts of relative permeability hysteresis, wettability, and injection/withdrawal schemes on underground hydrogen storage in saline aquifers', *Fuel*, vol. 333, 126516. <https://doi.org/10.1016/j.fuel.2022.126516>

Digital Object Identifier (DOI):

[10.1016/j.fuel.2022.126516](https://doi.org/10.1016/j.fuel.2022.126516)

Link:

[Link to publication record in Edinburgh Research Explorer](#)

Document Version:

Peer reviewed version

Published In:

Fuel

General rights

Copyright for the publications made accessible via the Edinburgh Research Explorer is retained by the author(s) and / or other copyright owners and it is a condition of accessing these publications that users recognise and abide by the legal requirements associated with these rights.

Take down policy

The University of Edinburgh has made every reasonable effort to ensure that Edinburgh Research Explorer content complies with UK legislation. If you believe that the public display of this file breaches copyright please contact openaccess@ed.ac.uk providing details, and we will remove access to the work immediately and investigate your claim.



1 **Impacts of relative permeability hysteresis, wettability, and injection/withdrawal**
2 **schemes on underground hydrogen storage in saline aquifers**

3 Bin Pan ¹, Kai Liu ¹, Bo Ren ², Mingshan Zhang ³, Yang Ju ⁴, Jianwei Gu ⁵, Xueying
4 Zhang ⁶, Christopher R. Clarkson ⁷, Katriona Edlmann ⁸, Weiyao Zhu ^{1*}, and Stefan
5 Iglauer ^{9,10}

6 *¹School of Civil and Resource Engineering, University of Science and Technology*
7 *Beijing, No. 30, Xueyuan Road, Beijing, 10083, China*

8 *²Bureau of Economic Geology, The University of Texas at Austin, 10611 Exploration*
9 *Way, Austin, TX 78758, US*

10 *³Key Laboratory of Ministry of Education on Safe Mining of Deep Metal Mines, School*
11 *of Resources and Civil Engineering, Northeastern University, Shenyang 110819, China*

12 *⁴State Key Laboratory of Coal Resources and Safe Mining, China University of Mining*
13 *and Technology at Beijing, D11 Xueyuan Road, Beijing 100083, China*

14 *⁵School of Petroleum Engineering, China University of Petroleum (East China), No. 66,*
15 *Changjiang West Road, Qingdao, China*

16 *⁶PetroChina Huabei Oilfield Company, Hebei, 062552, China*

17 *⁷Department of Geoscience, University of Calgary, Calgary, AB, T2N 1N4, Canada*

18 *⁸School of Geosciences, University of Edinburgh, Grant Institute, Edinburgh, UK*

19 *⁹School of Engineering, Edith Cowan University, 270 Joondalup Drive, Joondalup,*
20 *Australia*

21 *¹⁰Centre for Sustainable Energy and Resources, Edith Cowan University, 270*
22 *Joondalup Drive, Joondalup, Australia*

23

24 **Abstract**

25 Underground hydrogen storage (UHS) is a key strategy in the implementation of
26 a large-scale hydrogen (H_2) economy and promotion of renewable energy
27 development/utilization. For UHS in water-wet saline aquifers, H_2 displaces *in-situ*
28 brine during injection; during well shut-in and H_2 withdrawal, brine imbibes back into
29 the flow paths where it displaces some H_2 . These processes are influenced by H_2 -brine
30 transport physics, H_2 -brine-rock interactions and injection/withdrawal schemes, which,
31 in turn, determine H_2 storage capacities and injection/withdrawal efficiency. However,
32 these effects are poorly understood. Therefore, this work focuses on the impact of
33 relative permeability hysteresis (RPH), wettability, and H_2 withdrawal rate on UHS
34 performance in a saline aquifer. Furthermore, differences between UHS and CO_2 geo-
35 storage (CGS) are examined.

36 The primary findings include: 1) RPH results in a smaller H_2 withdrawal factor
37 (H_{2-WF}), but a larger H_2 withdrawal purity (H_{2-WP}); 2) H_{2-WF} increases with rock
38 hydrophobicity, while H_{2-WP} is mostly insensitive to rock wettability; 3) under
39 similar storage conditions, H_{2-WF} and H_{2-WP} are approximately 10% less than
40 CO_{2-WF} and CO_{2-WP} .

41 These insights demonstrate the significance of RPH and rock wettability on UHS
42 performance and provides guidance on H_2 injection/withdrawal scheme optimization.
43 This study aids in the implementation of an industry-scale hydrogen economy.

44

45 **Keywords:** Underground hydrogen storage; Saline aquifers; Relative permeability
46 hysteresis; Wettability; Injection/withdrawal scheme.

47

48 **1. Introduction**

49 Commercial development of renewable and sustainable energy resources are
50 required to accelerate energy transition, mitigate global warming, and accomplish
51 carbon neutrality [1–3]. However, these energy resources (e.g., wind, solar, and tide)
52 are time-, season-, weather- and/or region- dependent, which limits their stability,
53 reliability and large-scale economic implementation [4–6]. To overcome these
54 drawbacks, underground hydrogen storage (UHS) is considered as a promising solution
55 [7–11]. When energy supply is larger than energy demand, excess renewable and
56 sustainable energy can be converted to hydrogen (H₂) through water electrolysis as a
57 green energy carrier, and the H₂ can be injected into the subsurface for storage; when
58 energy demand is high, H₂ can be withdrawn again from the subsurface for usage [12–
59 17]. Potential subsurface storage sites include deep coal seams [18,19], depleted
60 hydrocarbon reservoirs [20,21], aquifers [22,23] and salt caverns [15,24]. Salt caverns
61 are suitable for frequent cyclic H₂ injection and withdrawal, but salt cavern storage
62 capacities are usually small (around $50 \times 10^4 \text{ Sm}^3$ [15,24,25]). Depleted
63 hydrocarbon reservoirs are often well characterized with the necessary geological
64 information, and substantial surface/subsurface infrastructure are in place [20,21].
65 However, microbial activity may be high, which causes both serious H₂ loss and H₂
66 purity reduction (e.g. via the reactions $\text{C}_2\text{H}_6 + \text{H}_2 \rightarrow 2 \text{CH}_4$ or $\text{H}_2 + \text{S} \rightarrow \text{H}_2\text{S}$

67 [8,16,26]). In contrast, saline aquifers have the largest storage capacity and relatively
68 weak microbial reactions, and thus attract significant attention [7,27]. Heinemann et al.
69 [7] discussed the scientific challenges to enabling large-scale hydrogen storage in saline
70 reservoirs while Pan et al. [27] reviewed all available experimental data related to UHS
71 in saline aquifers.

72 Numerical simulation is a cost-effective and rapid method for large-scale UHS
73 evaluation, which should be conducted prior to field-scale pilot tests. Pfeiffer et al.
74 [28,29] used numerical simulations to predict UHS performance in the Rhaetian deposit,
75 Germany, and the results demonstrated that up to $7700 \times 10^4 \text{ Sm}^3$ (equal to 245 MW
76 electricity) could be stored. Feldmann et al. [30] simulated 5 years of continuous H_2
77 injection and subsequent 5 years of seasonal cyclic H_2 injection/withdrawal into a
78 depleted gas reservoir; the authors found that the H_2 withdrawal purity (H_{2-WP}) and
79 withdrawal factor (H_{2-WF}) reached 82% - 85% and 39%, respectively. Sainz-Garcia et
80 al. [22] conducted a three-dimensional multiphase numerical simulation for three
81 annual H_2 injection/withdrawal cycles in Castilla-Leon, Spain. The stored H_2 (67400
82 $\times 10^4 \text{ Sm}^3$) was able to supply 15% of the electric consumption for a population of
83 175,000 over 3 months. Additionally, Lubon and Tarkowski [23] utilized numerical
84 simulations to predict seasonal H_2 cyclic injection/withdrawal scenarios in a deep
85 aquifer at Suliszewo, Poland - it was discovered that water coning was the main obstacle
86 for UHS performance. Recently, Heinemann et al. [11] investigated the role of cushion
87 gas for H_2 injection and withdrawal in saline aquifers, demonstrating that the produced

88 H₂ was equal to 1.625 TWH from a three dimensional anticline reservoir model with
89 the ratio of cushion gas to working gas at 1.27 [11].

90 In the above-mentioned UHS simulations, either CO₂-brine relative permeability
91 curves were used as input parameters [11,28,29], or H₂-brine relative permeability
92 hysteresis (RPH) was not considered [22,23,30] (though CO₂ RPH strongly influences
93 capillary CO₂ trapping in saline reservoirs in CGS schemes [31]). To mitigate this
94 uncertainty, and to address the fact that H₂ is a very different molecule than CH₄ or CO₂
95 [27,32], UHS reservoir simulations with real H₂ input parameters and H₂ transport
96 physics are required.

97 Therefore herein, the impact of RPH, rock-H₂ wettability, and
98 injection/withdrawal schemes on UHS performance in saline aquifers is systematically
99 evaluated. Further, the acquired UHS results are compared with CGS data. This work
100 will provide important information supporting large-scale UHS implementation and the
101 decarbonization of energy supply chains.

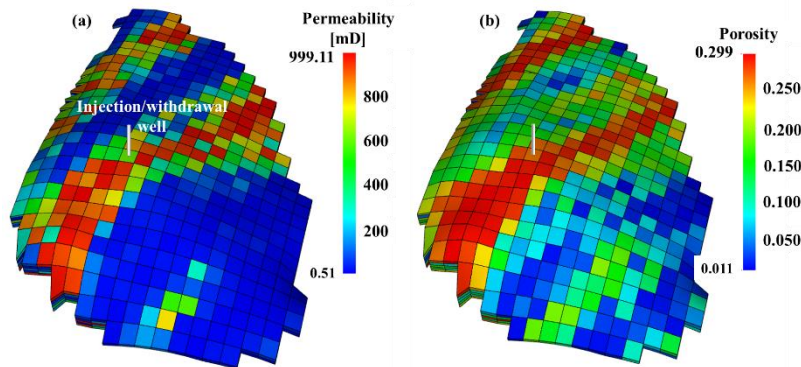
102

103 **2. Methodology**

104 **2.1 Geological model**

105 The commercial reservoir simulator IMEX from Computer Modelling Group
106 (CMG) was used to simulate UHS in a synthetic PUNQ-S3 geological model. This
107 simulation is based on the classic black-oil model following the mass conservation
108 principles [33]. PUNQ-S3 is a three-dimensional, geometrically complicated and
109 heterogeneous geological model (a central dome + 5 layers of sand/shale) [34]. This

110 model was previously used for oil production forecasting [34] and CO₂ geo-storage
111 simulation [31]. The average aquifer thickness is 15 m, and the entire domain is
112 discretized into 19 × 28 × 5 grid blocks (1761 of them active). Each cell has a length
113 of 180 m in the horizontal direction. The average horizontal permeability and porosity
114 are 100 mD and 0.2, respectively, with their spatial distributions shown in **Figure 1**.



115
116 **Figure 1.** (a) Horizontal permeability and (b) porosity distributions in the PUNQ-S3
117 geological model (Modified after [31]). For simplicity, only one well was used for gas
118 injection and withdrawal.

119

120 A single well was drilled at the structurally highest location for gas injection and
121 withdrawal. Similar to [31], the pore volume around the geological boundaries is set
122 ~1000 times larger than the area of interest so that *in-situ* brine could be displaced
123 during the gas injection; the displaced brine is imbibed back again during well shut-in
124 (in case of water-wet rock) and simultaneously pumped out of the subsurface with gas
125 during gas withdrawal.

126

127 2.2 Input parameters

128 Information about H₂ density, H₂ viscosity and H₂ expansion factor at UHS
129 conditions are tabulated in **Table 1**. Currently, only one H₂-brine relative permeability

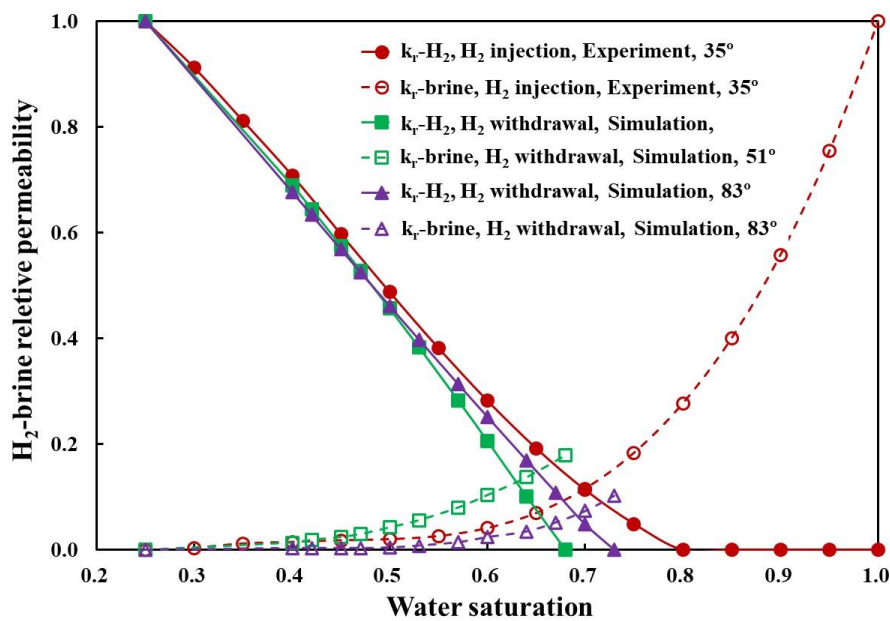
130 curve was measured for the process of H₂ injection into a brine saturated water-wet
 131 sandstone [35] (**Figure 2**). Using pore network modelling, H₂-brine relative
 132 permeability curves (for drainage and imbibition) were also predicted for additional
 133 rock wettabilities [i.e., brine contact angles (θ) of 51° and 83°] [36] (**Figure 2**).
 134 Information about CO₂ properties and relative permeability curves (which were
 135 collected from previous literature [31]) are not shown here for simplicity.

136

137 **Table 1.** H₂ properties at 40 °C and various pressures (compiled from [7,27]).

Pressure [MPa]	Density [kg/m ³]	Expansion factor [-]	Viscosity [mPa·s]
0.1	0.089	1	0.0092
10	8	89.9	0.0094
20	14	157.3	0.0096
30	20	224.7	0.0098
40	24	269.7	0.01
50	29	325.8	0.0104

138



139

140 **Figure 2.** H₂-brine relative permeability curves (modified after [35,36]; curve fitting
 141 was conducted to smooth the raw experimental and simulation data based on the least
 142 squares method). Experimental data is from [30]; simulated curves using pore network
 143 modeling are from [31].

144

145 2.3 Simulation scenarios

146 Four separate scenarios were simulated to explore the impact of RPH, rock
 147 wettability, and injection/withdrawal scheme on UHS performance, **Table 2.** In addition,
 148 two scenarios were simulated for CGS to provide a comparison.

149

150 **Table 2.** Scenarios simulated in this work (NA means that CO₂ wettability was
 151 unknown in the simulations).

Gas	Case	Relative permeability hysteresis	Wettability	Injection/withdrawal scheme
H ₂	1 (base case)	No	35°	a. Injection at 50×10^4 Sm ³ /day for 9 months; well shut-in for 3 months b. Withdrawal at 100×10^4 Sm ³ /day for 3 months; injection at 50×10^4 Sm ³ /day for 6 months; well shut-in for 3 months c. Repeat b for 4 cycles
	2	Yes	51°	Same as case 1
	3	Yes	83°	Same as above
	4	Yes	51°	a. Injection at 50×10^4 Sm ³ /day for 9 months; well shut-in for 3 months b. Withdrawal at 200×10^4 Sm ³ /day for 3 months; injection at 50×10^4 Sm ³ /day for 6 months; well shut-in for 3 months c. Repeat b for 4 cycles
CO ₂	5 (base case)	No	NA	a. Injection at 50×10^4 Sm ³ /day for 9 months; well shut-in for 3 months b. Withdrawal at 100×10^4 Sm ³ /day for 3 months; injection at 50×10^4 Sm ³ /day for 6 months; well shut-in for 3 months c. Repeat b for 4 cycles
	6	Yes	NA	Same as case 5

152

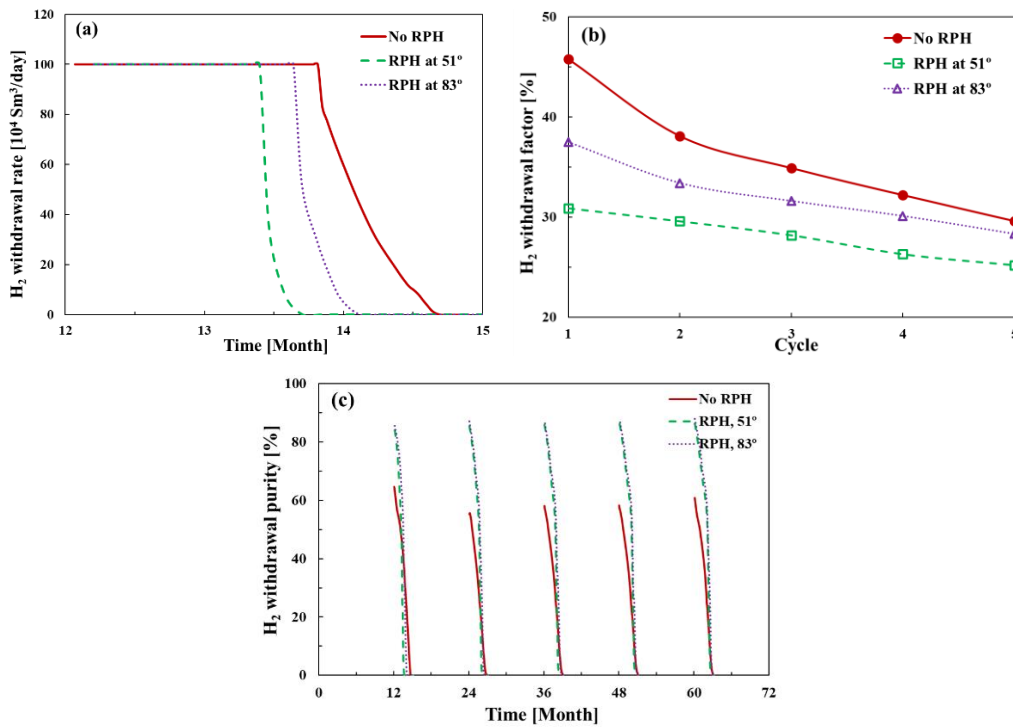
153 3 Results and discussion

154 3.1 Impact of relative permeability hysteresis and wettability

155 For UHS, H₂ injection into a water-wet aquifer is dominated by the forced
156 drainage (of the resident formation water), while H₂ withdrawal is dominated by the
157 spontaneous and forced imbibition [37,38]. Therefore, it is necessary to assess the
158 impact of RPH and rock wettability on UHS performance.

159

160



161

162 **Figure 3.** Effect of relative permeability hysteresis and rock wettability on the (a) actual
163 H₂ withdrawal rate during the 1st withdrawal cycle, (b) H₂ withdrawal factor (the ratio
164 of the accumulated H₂ withdrawal volume during a specific H₂ withdrawal cycle to the
165 total H₂ in-place volume prior to this withdrawal cycle) and (c) H₂ withdrawal purity
166 (the ratio of H₂ withdrawal mass to water production mass) at the prescribed withdrawal
167 rate of $100 \times 10^4 \text{ Sm}^3/\text{day}$.

168

169 RPH and a strongly water-wet state cause the actual H_2 withdrawal rate (H_{2-WR})
170 to deviate from the prescribed H_{2-WR} value and to reach zero earlier, **Figure 3(a)**.
171 During the 1st H_2 withdrawal cycle, the actual H_{2-WR} started to deviate from the
172 prescribed $100 \times 10^4 \text{ Sm}^3/\text{day}$ on the 54th, 36th and 45th day, while it reached zero on
173 the 81st, 49th and 62nd day, for the case of no RPH, case with RPH at $\theta = 51^\circ$, and the
174 case with RPH at $\theta = 83^\circ$, respectively. Further, by the end of each withdrawal cycle,
175 the H_2 withdrawal factor (H_{2-WF} , the ratio of the accumulated H_2 withdrawal volume
176 during a specific H_2 withdrawal cycle to the total H_2 in-place volume prior to this
177 withdrawal cycle) follows the order: case with no RPH > case with RPH at $\theta = 83^\circ$ >
178 case with RPH at $\theta = 51^\circ$. H_{2-WF} was 38%, 33% and 30%, respectively for the
179 above-mentioned three scenarios at the end of the 2nd withdrawal cycle, **Figure 3(b)**.
180 Moreover, at the beginning of each H_2 withdrawal cycle, RPH causes a larger H_2
181 withdrawal purity (H_{2-WP} , the ratio of H_2 withdrawal mass to water production mass)
182 than without RPH (e.g., 86% - 88% versus 55% - 65%), though the wettability impact
183 is insignificant, **Figure 3(c)**. In addition, with the H_2 withdrawal cycle increase, H_{2-WF}
184 decreased at the end of each cycle of withdrawal, while H_{2-WP} increased at the
185 beginning of each cycle of withdrawal, **Figure 3(b)** and **(c)**, consistent with the previous
186 literature study [28].

187 Note that RPH and rock wettability influence pore-scale gas-brine two phase flow
188 characteristics and therefore determine reservoir-scale gas injection/withdrawal
189 efficiency [38–43]. In the absence of RPH, the injected gas exists as a continuous gas
190 plume, and capillary trapping is relatively weak [31]. If RPH is present, the trailing

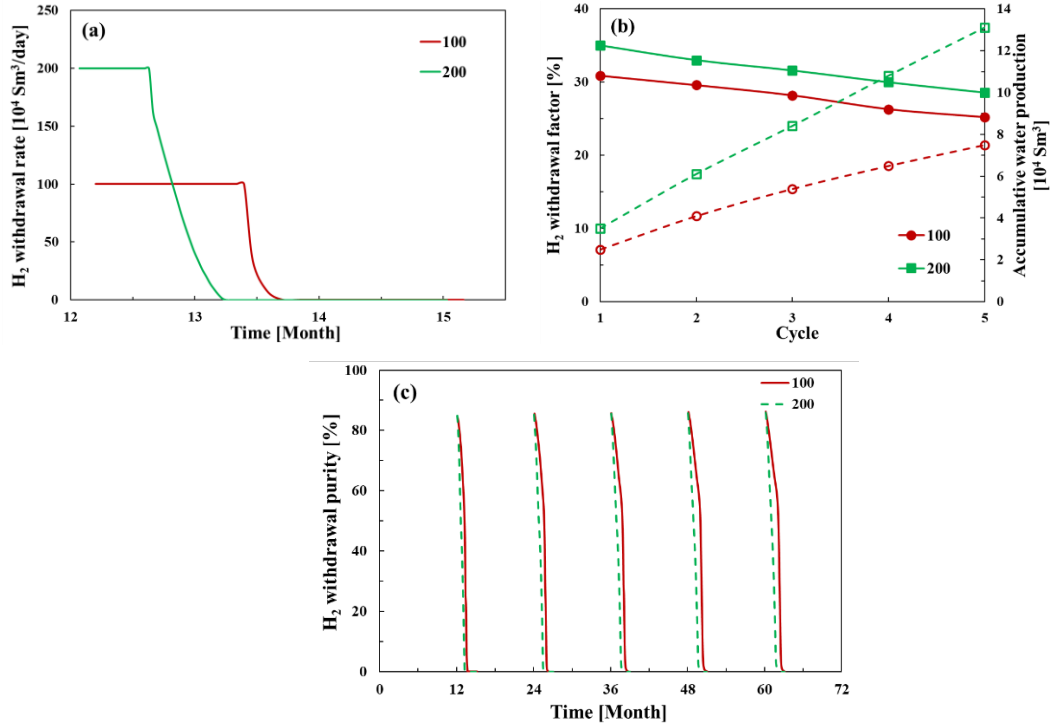
191 edges of the gas plumes tend to convert into discontinuous phases, and capillary
192 trapping are relatively strong (which is favorable for CGS because of reduced leakage
193 risk) – however, it is unfavorable for UHS because of the more difficult gas re-
194 mobilization [27]. Therefore, H_{2-WF} was higher in the absence of RPH. Further, a
195 more water-wet state leads to more snap off events [44,45], and therefore a more serious
196 H_2 loss and a smaller H_{2-WF} . Moreover, during well shut-in, discontinuous H_2 bubbles
197 can exert strong resistance for the spontaneous imbibition of *in-situ* formation brine
198 [46,47] – therefore, if RPH is present, the initial H_2 concentration is higher around the
199 wellbore region (which again results in a larger H_{2-WP} at the beginning of each H_2
200 withdrawal cycle). The observed H_{2-WF} and H_{2-WP} response to the withdrawal
201 cycle is because 1) at the end of each H_2 injection cycle, more H_2 will be in place than
202 the earlier injection cycle; and 2) at the end of each H_2 withdrawal cycle, more H_2 will
203 be lost to the subsurface than the earlier withdrawal cycle [28].

204

205 **3.2 Impact of H_2 withdrawal rate**

206 To operate a field-scale UHS project efficiently, the H_2 injection/withdrawal
207 scheme [7] should be optimized, especially H_{2-WR} . Therefore, the impact of H_{2-WR}
208 on UHS performance was investigated in this section.

209



210

211

212 **Figure 4.** Effect of the prescribed H₂ withdrawal rate on (a) actual H₂ withdrawal rate
 213 during the 1st withdrawal cycle, (b) H₂ withdrawal factor and (c) H₂ withdrawal purity
 214 for the case of relative permeability hysteresis and brine contact angle of 51°.

215

216 Clearly, a larger prescribed H_{2-WR} causes the actual H_{2-WR} to deviate from the
 217 pre-set value and reach zero earlier in the simulated cases, **Figure 4(a) and (b)**. For
 218 example, during the 1st H₂ withdrawal cycle (for the prescribed $H_{2-WR} = 100 \times 10^4$
 219 Sm³/day and $H_{2-WR} = 200 \times 10^4$ Sm³/day), the actual H_{2-WR} started to deviate
 220 from the prescribed value on the 38th and 18th day, respectively, while it reached zero
 221 on the 50th and 36th day, respectively. This is due to the faster pressure depletion caused
 222 by the larger H_{2-WR} [48]. Therefore, it is suggested that sufficient H₂ is stored and
 223 sufficiently high reservoir pressure is maintained for continuous H₂ withdrawal at an
 224 expected withdrawal rate. Furthermore, a larger H_{2-WR} caused a larger H_{2-WF} and a
 225 more serious water production problem. For example, for the prescribed $H_{2-WR} =$
 226 100×10^4 Sm³/day and $H_{2-WR} = 200 \times 10^4$ Sm³/day, by the end of the 5th H₂

227 withdrawal cycle, H_{2-WF} was 25% and 29% respectively, and cumulative water
228 production reached $7.5 \times 10^4 \text{ Sm}^3$ and $13.1 \times 10^4 \text{ Sm}^3$, respectively.

229 In principle, larger H_2 injection rates result in higher viscous forces, which can
230 override capillary forces (analogue to CO_2 flooding [49]), and suppress lateral H_2
231 migration beneath the caprock, resulting in a larger H_{2-WF} [31]. However, to avoid
232 water production problems, an optimized H_2 withdrawal rate is required; to determine
233 this optimum H_2 withdrawal scheme, it is suggested that a balance between initial gas
234 in place, transient H_2 demand, and gas purification/separation ability should all be
235 considered [23].

236

237 **3.3 Impact of gas type**

238 During the past decades, CGS has been investigated comprehensively (e.g.,
239 [31,40,42,43,50–54]). In contrast, UHS is a relatively new technology which is still in
240 its infancy [27,55–57]. Whether previous learnings from CGS can be directly used in
241 UHS is still uncertain. Therefore, in this section, UHS and CGS are compared (under
242 the prescribed gas withdrawal rate of $100 \times 10^4 \text{ Sm}^3/\text{day}$ and RPH conditions, **Table**
243 **3** and **Figure 5**).

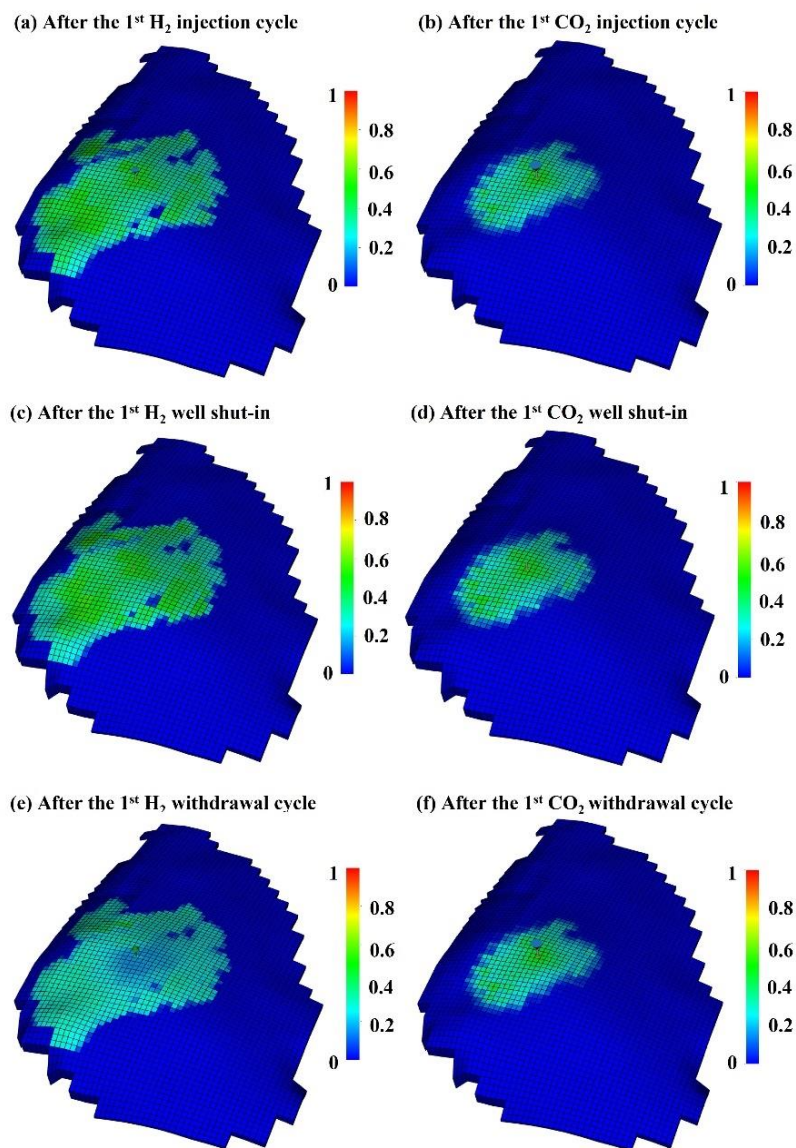
244

245 **Table 3.** Comparisons between underground hydrogen storage (UHS) and CO_2 geo-
246 storage (CGS) during the first cycle of withdrawal, under the prescribed gas withdrawal
247 rate of $100 \times 10^4 \text{ Sm}^3/\text{day}$ and relative permeability hysteresis conditions.

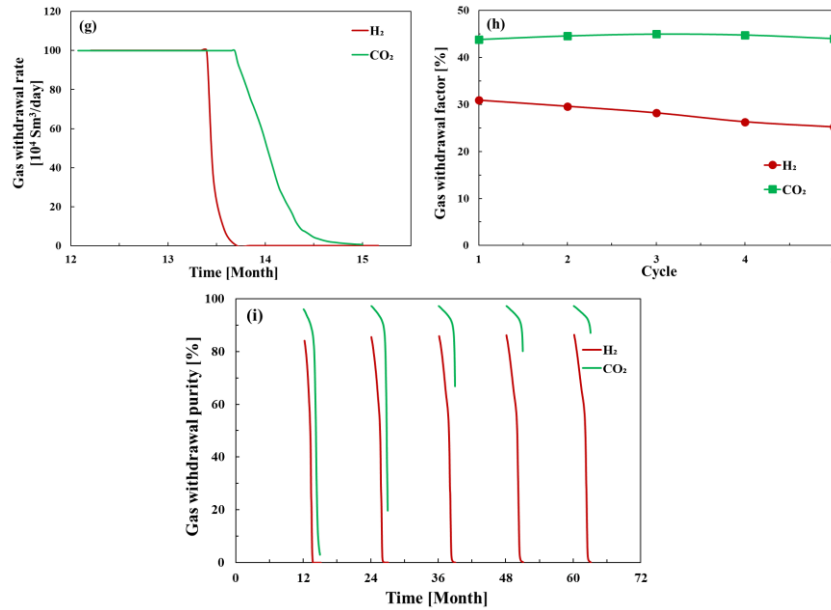
Gas	Plume areal coverage	Deviation from the prescribed withdrawal rate	Withdrawal factor by the end	Withdrawal purity at the beginning
UHS	Large: 35.22 km ² ; 30.5%	Early: 38 days	Low: 31%	Low: 84%
CGS	Small: 14.58 km ² ; 12.6%	Late: 50 days	High: 44%	High: 96%

248

249



250



251

252

253 **Figure 5.** (a-f) Gas saturation distribution during the 1st H_2 storage cycle; (g) the actual
 254 gas withdrawal rate during the 1st withdrawal cycle; (h) gas withdrawal factor during
 255 the continuous 5 withdrawal cycles and (i) gas withdrawal purity during the continuous
 256 5 withdrawal cycles under the prescribed withdrawal rate of $100 \times 10^4 \text{ Sm}^3/\text{day}$ and
 257 relative permeability hysteresis conditions.

258

259 Clearly, UHS and CGS exhibit significant differences in gas saturation distribution,

260 actual gas withdrawal rate, gas withdrawal factor and gas purity, **Table 3** and **Figure 5**.

261 After the initial gas injection for 9 months, the H_2 plume was $\sim 2 - 5$ times larger than

262 CO_2 , **Figure 5(a)** and **(b)** - this difference is caused by different gas viscosity and

263 diffusivity [27]; after a well shut-in for 3 months, H_2 migrated significantly upward and

264 accumulated beneath the caprock, while CO_2 only migrated slightly upward, **Figure**

265 **5(c)** and **(d)** - this was mainly caused by the difference in gas-brine density [27,58].

266 Furthermore, as shown in **Table 3**, **Figure 5(h)** and **(i)**, in the same timeframe, H_{2-WF}

267 and H_{2-WP} were smaller than CO_{2-WF} and CO_{2-WP} .

268 Note that sandstone rocks are more water-wet in a H_2 environment than in a CO_2

269 environment [55,57,59,60], therefore gas bubble snap-off is more favored for H_2 than

270 for CO₂, which has led lower H_{2-WF} than CO_{2-WF} [61,62]). Meanwhile, especially
271 during the gas injection stage, viscous fingering was predicted to be more pronounced
272 for H₂ than for CO₂ [27], and that H₂ moves farther away from the wellbore region than
273 CO₂ [57].

274

275 **4 Conclusions and Recommendations**

276 Underground hydrogen storage (UHS) is a promising technology which could aid
277 the development of a large-scale hydrogen economy [12–17]. For UHS in saline
278 aquifers, H₂-multi-cycle injection/withdrawal schemes are influenced by the energy
279 supply and demand [23,63]. H₂-brine two phase flow physics, and H₂-brine-rock
280 interactions determine UHS performance [7,27]. Therefore, in this work, the impact of
281 relative permeability hysteresis, rock wettability, and injection/withdrawal schemes are
282 systematically studied, and the results for UHS are then compared with those for CO₂
283 geo-storage (CGS). The following conclusions are reached:

284

- 285 1) H₂-brine relative permeability hysteresis results in a lower H₂ withdrawal
286 factor, but a higher purity of withdrawn gas.
- 287 2) More water-wet rocks have lower H₂ withdrawal efficiencies.
- 288 3) Larger H₂ withdrawal rates increase H₂ withdrawal efficiency, but also
289 increase water production.
- 290 4) UHS and CGS demonstrate significant differences and direct correlations
291 should be avoided.

292

293 This study provides important information to aid in the implementation of a large-
294 scale hydrogen economy, and therefore also supports the decarbonization of energy
295 supply chains. For future work, it is suggested to further analyze the pore-scale H₂-
296 brine two phase flow physics, and to establish a better understanding of meso-scale
297 parameters (such as the H₂-brine relative permeabilities for cyclic drainage and
298 imbibition processes and how they vary with wettability). Such improved input data
299 leads directly to improved prediction of UHS performance [64,65].

300

301 **Acknowledgements**

302 Bin Pan thanks the initiative funding from the University of Science and
303 Technology Beijing. Weiyao Zhu thanks the funding support from the National Natural
304 Science Foundation of China (No. 51974013 and No. 11372033) and Open Research
305 Foundation (NEPU-EOR-2019-003). Yang Ju acknowledges the funding support from
306 the National Natural Science Foundation of China (No. 52121003). Christopher R.
307 Clarkson thanks the sponsors of the Tight Oil Consortium (TOC) and Orintiv and Shell
308 for support of his Chair position in Unconventional Gas and Light Oil Research in the
309 Department of Geoscience at the University of Calgary. Stefan Iglauer would like to
310 thank the Australian Research Council for financial support (under grant
311 DP220102907).

312

313 **References**

314 [1] Hosseini SE, Wahid MA. Hydrogen production from renewable and sustainable

- 315 energy resources: Promising green energy carrier for clean development. *Renew*
316 *Sustain Energy Rev* 2016;57:850–66.
317 <https://doi.org/10.1016/J.RSER.2015.12.112>.
- 318 [2] Lau LC, Lee KT, Mohamed AR. Global warming mitigation and renewable
319 energy policy development from the Kyoto Protocol to the Copenhagen
320 Accord—A comment. *Renew Sustain Energy Rev* 2012;16:5280–4.
321 <https://doi.org/10.1016/J.RSER.2012.04.006>.
- 322 [3] Lam PTI, Law AOK. Crowdfunding for renewable and sustainable energy
323 projects: An exploratory case study approach. *Renew Sustain Energy Rev*
324 2016;60:11–20. <https://doi.org/10.1016/J.RSER.2016.01.046>.
- 325 [4] Rourke FO, Boyle F, Reynolds A. Renewable energy resources and technologies
326 applicable to Ireland. *Renew Sustain Energy Rev* 2009;13:1975–84.
327 <https://doi.org/10.1016/J.RSER.2009.01.014>.
- 328 [5] Bhuiyan MRA, Mamur H, Begum J. A brief review on renewable and sustainable
329 energy resources in Bangladesh. *Clean Eng Technol* 2021;4:100208.
330 <https://doi.org/10.1016/J.CLET.2021.100208>.
- 331 [6] Widén J, Carpman N, Castellucci V, Lingfors D, Olauson J, Remouit F, et al.
332 Variability assessment and forecasting of renewables: A review for solar, wind,
333 wave and tidal resources. *Renew Sustain Energy Rev* 2015;44:356–75.
334 <https://doi.org/10.1016/J.RSER.2014.12.019>.
- 335 [7] Heinemann N, Alcalde J, Miodic JM, Hangx SJT, Kallmeyer J, Ostertag-
336 Henning C, et al. Enabling large-scale hydrogen storage in porous media – the

- 337 scientific challenges. *Energy Environ Sci* 2021;14:853–64.
338 <https://doi.org/10.1039/d0ee03536j>.
- 339 [8] Thaysen EM, McMahon S, Strobel GJ, Butler IB, Ngwenya BT, Heinemann N,
340 et al. Estimating microbial growth and hydrogen consumption in hydrogen
341 storage in porous media. *Renew Sustain Energy Rev* 2021;151:111481.
342 <https://doi.org/10.1016/J.RSER.2021.111481>.
- 343 [9] Miocic JM, Heinemann N, Edlmann K, Scafidi J, Molaei F, Alcalde J.
344 Underground hydrogen storage: a review. *Geol Soc London* 2022;528.
- 345 [10] Rezaei A, Hassanpouryouzband A, Molnar I, Derikvand Z, Haszeldine S,
346 Edlmann K. Relative permeability of hydrogen and aqueous brines in sandstones
347 and carbonates at reservoir conditions. *Geophys Res Lett* 2022;49.
- 348 [11] Heinemann N, Scafidi J, Pickup G, Thaysen EM, Hassanpouryouzband A,
349 Wilkinson M, et al. Hydrogen storage in saline aquifers: The role of cushion gas
350 for injection and production. *Int J Hydrogen Energy* 2021;46:39284–96.
- 351 [12] Lankof L, Tarkowski R. Assessment of the potential for underground hydrogen
352 storage in bedded salt formation. *Int J Hydrogen Energy* 2020;45:19479–92.
353 <https://doi.org/10.1016/j.ijhydene.2020.05.024>.
- 354 [13] Tarkowski R. Underground hydrogen storage: Characteristics and prospects.
355 *Renew Sustain Energy Rev* 2019;105:86–94.
356 <https://doi.org/10.1016/j.rser.2019.01.051>.
- 357 [14] Tarkowski R, Czapowski G. Salt domes in Poland – Potential sites for hydrogen
358 storage in caverns. *Int J Hydrogen Energy* 2018;43:21414–27.

- 359 <https://doi.org/10.1016/J.IJHYDENE.2018.09.212>.
- 360 [15] Ozarslan A. Large-scale hydrogen energy storage in salt caverns. *Int J Hydrogen*
361 *Energy* 2012;37:14265–77. <https://doi.org/10.1016/j.ijhydene.2012.07.111>.
- 362 [16] Carden PO, Paterson L. Physical, chemical and energy aspects of underground
363 hydrogen storage. *Int J Hydrogen Energy* 1979;4:559–69.
364 [https://doi.org/10.1016/0360-3199\(79\)90083-1](https://doi.org/10.1016/0360-3199(79)90083-1).
- 365 [17] Qiu Y, Zhou S, Wang J, Chou J, Fang Y, Pan G, et al. Feasibility analysis of
366 utilising underground hydrogen storage facilities in integrated energy system:
367 Case studies in China. *Appl Energy* 2020;269:115140.
368 <https://doi.org/10.1016/j.apenergy.2020.115140>.
- 369 [18] Sedev R, Akhondzadeh H, Ali M, Keshavarz A, Iglauer S. Contact Angles of a
370 Brine on a Bituminous Coal in Compressed Hydrogen. *Geophys Res Lett*
371 2022;49:e2022GL098261. <https://doi.org/10.1029/2022GL098261>.
- 372 [19] Iglauer S, Akhondzadeh H, Abid H, Paluszny A, Keshavarz A, Ali M, et al.
373 Hydrogen flooding of a coal core: Effect on Coal Swelling. *Geophys Res Lett*
374 2022;49:e2021GL096873. <https://doi.org/10.1029/2021GL096873>.
- 375 [20] Kanaani M, Sedae B, Asadian-Pakfar M. Role of cushion gas on underground
376 hydrogen storage in depleted oil reservoirs. *J Energy Storage* 2022;45:103783.
377 <https://doi.org/10.1016/J.EST.2021.103783>.
- 378 [21] Amid A, Mignard D, Wilkinson M. Seasonal storage of hydrogen in a depleted
379 natural gas reservoir. *Int J Hydrogen Energy* 2016;41:5549–58.
380 <https://doi.org/10.1016/j.ijhydene.2016.02.036>.

- 381 [22] Sainz-Garcia A, Abarca E, Rubi V, Grandia F. Assessment of feasible strategies
382 for seasonal underground hydrogen storage in a saline aquifer. *Int J Hydrogen*
383 *Energy* 2017;42:16657–66. <https://doi.org/10.1016/j.ijhydene.2017.05.076>.
- 384 [23] Luboń K, Tarkowski R. Numerical simulation of hydrogen injection and
385 withdrawal to and from a deep aquifer in NW Poland. *Int J Hydrogen Energy*
386 2020;45:2068–83. <https://doi.org/10.1016/j.ijhydene.2019.11.055>.
- 387 [24] Caglayan DG, Weber N, Heinrichs HU, Linßen J, Robinius M, Kukla PA, et al.
388 Technical potential of salt caverns for hydrogen storage in Europe. *Int J*
389 *Hydrogen Energy* 2020;45:6793–805.
390 <https://doi.org/10.1016/J.IJHYDENE.2019.12.161>.
- 391 [25] Portarapillo M, Di Benedetto A. Risk assessment of the large-scale hydrogen
392 storage in salt caverns. *Energies* 2021, 14, 2856 2021;14:2856.
393 <https://doi.org/10.3390/EN14102856>.
- 394 [26] Walters AB, Walters, B. A. Technical and environmental aspects of underground
395 hydrogen storage. *Whe2* 1976;2:2B_65-2B_79.
- 396 [27] Pan B, Yin X, Ju Y, Iglauer S. Underground hydrogen storage: influencing
397 parameters and future outlook. *Adv Colloid Interface Sci* 2021, 294, 102473.
- 398 [28] Pfeiffer WT, Bauer S. Subsurface Porous Media Hydrogen Storage – Scenario
399 Development and Simulation. *Energy Procedia* 2015;76:565–72.
400 <https://doi.org/10.1016/J.EGYPRO.2015.07.872>.
- 401 [29] Pfeiffer WT, Beyer C, Bauer S. Hydrogen storage in a heterogeneous sandstone
402 formation: Dimensioning and induced hydraulic effects. *Pet Geosci*

- 403 2017;23:315–26. <https://doi.org/10.1144/PETGEO2016->
404 050/CITE/REFWORKS.
- 405 [30] Feldmann F, Hagemann B, Ganzer L, Panfilov M. Numerical simulation of
406 hydrodynamic and gas mixing processes in underground hydrogen storages.
407 Environ Earth Sci 2016;75:1–15. <https://doi.org/10.1007/S12665-016-5948->
408 Z/FIGURES/9.
- 409 [31] Juanes R, Spiteri EJ, Orr FM, Blunt MJ. Impact of relative permeability
410 hysteresis on geological CO₂ storage. Water Resour Res 2006;42:12418.
411 <https://doi.org/10.1029/2005WR004806>.
- 412 [32] Pan B, Ni T, Zhu W, Yang Y, Ju Y, Zhang L, et al. Mini review on wettability in
413 the methane-liquid-rock system at reservoir conditions: Implications for gas
414 recovery and geo-storage. Energy & Fuels 2022;36:4268–75.
- 415 [33] Aziz K, A S. Petroleum reservoir simulation. 1979.
- 416 [34] Floris FJT, Bush MD, Cuypers M, Roggero F, Syversveen AR. Methods for
417 quantifying the uncertainty of production forecasts: A comparative study. Pet
418 Geosci 2001;7:S87–96.
419 <https://doi.org/10.1144/PETGEO.7.S.S87/CITE/REFWORKS>.
- 420 [35] Yekta AE, Manceau JC, Gaboreau S, Pichavant M, Audigane P. Determination
421 of hydrogen–water relative permeability and capillary pressure in sandstone:
422 Application to underground hydrogen injection in sedimentary Formations.
423 Transp Porous Media 2018;122:333–56. <https://doi.org/10.1007/s11242-018->
424 1004-7.

- 425 [36] Hashemi L, Blunt M, Hajibeygi H. Pore-scale modelling and sensitivity analyses
426 of hydrogen-brine multiphase flow in geological porous media. *Sci Reports* 2021
427 111 2021;11:1–13. <https://doi.org/10.1038/s41598-021-87490-7>.
- 428 [37] Bachu S. Drainage and imbibition CO₂/brine relative permeability curves at in
429 situ conditions for sandstone formations in western Canada. *Energy Procedia*, 37,
430 2013, 4428–36. <https://doi.org/10.1016/j.egypro.2013.07.001>.
- 431 [38] Bennion DB, Bachu S. Drainage and imbibition relative permeability
432 relationships for supercritical CO₂/brine and H₂S/brine systems in intergranular
433 sandstone, carbonate, shale, and anhydrite rocks. *SPE Reserv Eval Eng*
434 2008;11:487–96. <https://doi.org/10.2118/99326-pa>.
- 435 [39] Krevor SCM, Pini R, Zuo L, Benson SM. Relative permeability and trapping of
436 CO₂ and water in sandstone rocks at reservoir conditions. *Water Resour Res*
437 2012;48. <https://doi.org/10.1029/2011WR010859>.
- 438 [40] Pan B, Li Y, Wang H, Jones F, Iglauer S. CO₂ and CH₄ wettabilities of organic-
439 rich shale. *Energy and Fuels* 2018;32:1914–22.
440 <https://doi.org/10.1021/acs.energyfuels.7b01147>.
- 441 [41] Pan B, Jones F, Huang Z, Yang Y, Li Y, Hejazi SH, et al. Methane (CH₄)
442 wettability of clay-coated quartz at reservoir conditions. *Energy and Fuels*
443 2019;33:788–95. <https://doi.org/10.1021/acs.energyfuels.8b03536>.
- 444 [42] Iglauer S, Pentland CH, Busch A. CO₂ wettability of seal and reservoir rocks and
445 the implications for carbon geo-sequestration. *Water Resour Res* 2015;51:729–
446 74. <https://doi.org/10.1002/2014WR015553>.

- 447 [43] Iglauer S, Paluszny A, Pentland CH, Blunt MJ. Residual CO₂ imaged with X-ray
448 micro-tomography. *Geophys Res Lett* 2011;38:n/a-n/a.
449 <https://doi.org/10.1029/2011GL049680>.
- 450 [44] Hu R, Wan J, Kim Y, Tokunaga TK. Wettability impact on supercritical CO₂
451 capillary trapping: Pore-scale visualization and quantification. *Water Resour Res*
452 2017;53:6377–94. <https://doi.org/10.1002/2017WR020721>.
- 453 [45] Hu R, Wan J, Yang Z, Chen Y, Tokunaga T. Wettability and flow rate impacts on
454 immiscible displacement: A theoretical model. *Geophys Res Lett* 2018;45:3077–
455 86. <https://doi.org/10.1002/2017GL076600>.
- 456 [46] Pan B, Clarkson CR, Younis A, Song C, Debuhr C, Ghanizadeh A, et al.
457 Fracturing fluid loss in unconventional reservoirs: evaluating the impact of
458 osmotic pressure and surfactant and methods to upscale results. *URTeC Tech*
459 2021:26–8. <https://doi.org/10.15530/URTEC-2021-5139>.
- 460 [47] Pan B, Clarkson CR, Younis A, Song C, Debuhr C, Ghanizadeh A, et al. New
461 methods to evaluate impacts of osmotic pressure and surfactant on fracturing
462 fluid loss and effect of contact angle on spontaneous imbibition data scaling in
463 unconventional reservoirs. *Fuel* 2022;328.
464 <https://doi.org/10.1016/j.fuel.2022.125328>.
- 465 [48] Clarkson CR. *Unconventional reservoir rate-transient analysis*. Elsevier; 2021.
- 466 [49] Jin X, Chao C, Edlmann K, Fan X. Understanding the interplay of capillary and
467 viscous forces in CO₂ core flooding experiments. *J Hydrol* 2022;606:127411.
- 468 [50] Wan J, Kim Y, Tokunaga TK. Contact angle measurement ambiguity in

- 469 supercritical CO₂-water-mineral systems: Mica as an example. *Int J Greenh Gas*
470 *Control* 2014;31:128–37. <https://doi.org/10.1016/j.ijggc.2014.09.029>.
- 471 [51] Wan J, Tokunaga TK, Ashby PD, Kim Y, Voltolini M, Gilbert B, et al.
472 Supercritical CO₂ uptake by nonswelling phyllosilicates. *Proc Natl Acad Sci U*
473 *S A* 2018;115:873–8. <https://doi.org/10.1073/pnas.1710853114>.
- 474 [52] Iglauer S. CO₂-water-rock wettability: Variability, influencing factors, and
475 implications for CO₂ geostorage. *Acc Chem Res* 2017;50:1134–42.
476 <https://doi.org/10.1021/acs.accounts.6b00602>.
- 477 [53] Pan B, Gong C, Wang X, Li Y, Iglauer S. The interfacial properties of clay-coated
478 quartz at reservoir conditions. *Fuel* 2020;262:116461.
479 <https://doi.org/10.1016/j.fuel.2019.116461>.
- 480 [54] Tenney CM, Cygan RT. Molecular simulation of carbon dioxide, brine, and clay
481 mineral interactions and determination of contact angles. *Environ Sci Technol*
482 2014;48:2035–42. <https://doi.org/10.1021/es404075k>.
- 483 [55] Ali M, Pan B, Yekeen N, Al-Anssari S, Al-Anazi A, Keshavarz A, et al.
484 Assessment of wettability and rock-fluid interfacial tension of caprock:
485 Implications for hydrogen and carbon dioxide geo-storage. *Int J Hydrogen*
486 *Energy* 2022. <https://doi.org/10.1016/J.IJHYDENE.2022.02.149>.
- 487 [56] Pan B, Yin X, Iglauer S. Rock-fluid interfacial tension at subsurface conditions:
488 Implications for H₂, CO₂ and natural gas geo-storage. *Int J Hydrogen Energy*
489 2021. <https://doi.org/10.1016/j.ijhydene.2021.05.067>.
- 490 [57] Pan B, Yin X, Zhu W, Yang Y, Ju Y, Yuan Y, et al. Theoretical study of brine

491 secondary imbibition in sandstone reservoirs: Implications for H₂, CH₄, and CO₂
492 geo-storage. Int J Hydrogen Energy 2022;47:18058–66.
493 <https://doi.org/10.1016/J.IJHYDENE.2022.03.275>.

494 [58] Ren B, Jerry J, Duncan I, Lake L. Buoyant flow of H₂ versus CO₂ in storage
495 aquifers. SPE Annu. Tech. Conf. Exhib. Houston, Texas, USA, Oct. 2022.

496 [59] Iglauer S, Ali M, Keshavarz A. Hydrogen wettability of sandstone reservoirs:
497 Implications for hydrogen geo-storage. Geophys Res Lett 2020.
498 <https://doi.org/10.1029/2020GL090814>.

499 [60] Ali M, Jha NK, Al-Yaseri A, Zhang Y, Iglauer S, Sarmadivaleh M. Hydrogen
500 wettability of quartz substrates exposed to organic acids; Implications for
501 hydrogen geo-storage in sandstone reservoirs. J Pet Sci Eng 2021;207:109081.
502 <https://doi.org/10.1016/J.PETROL.2021.109081>.

503 [61] Krevor S, Blunt MJ, Benson SM, Pentland CH, Reynolds C, Al-Menhali A, et al.
504 Capillary trapping for geologic carbon dioxide storage – From pore scale physics
505 to field scale implications. Int J Greenh Gas Control 2015;40:221–37.
506 <https://doi.org/10.1016/J.IJGGC.2015.04.006>.

507 [62] Lysy M, Ersland G, Fernø M. Pore-scale dynamics for underground porous
508 media hydrogen storage. Adv Water Resour 2022;163:104167.
509 <https://doi.org/10.1016/J.ADVWATRES.2022.104167>.

510 [63] Lysy M, Fernø M, Ersland G. Seasonal hydrogen storage in a depleted oil and
511 gas field. Int J Hydrogen Energy 2021;46:25160–74.
512 <https://doi.org/10.1016/J.IJHYDENE.2021.05.030>.

- 513 [64] Tarkowski R, Uliasz-Misiak B. Towards underground hydrogen storage: A
514 review of barriers. *Renew Sustain Energy Rev* 2022;162:112451.
515 <https://doi.org/10.1016/J.RSER.2022.112451>.
- 516 [65] van Rooijen W, Hashemi L, Boon M, Farajzadeh R, Hajibeygi H. Microfluidics-
517 based analysis of dynamic contact angles relevant for underground hydrogen
518 storage. *Adv Water Resour* 2022;164:104221.
519 <https://doi.org/10.1016/J.ADVWATRES.2022.104221>.
520